Requirement of neuronal- and cardiac-type sodium channels for murine sinoatrial node pacemaking

Ming Lei[1,*], Sandra A. Jones[2,*], Jie Liu[1], Matthew K. Lancaster[2], Simon S.-M. Fung[1], Halina Dobrzynski[2], Patrizia Camelliti[1], Sebastian K. G. Maier[3], Denis Noble[1] and Mark R. Boyett[2]

[1] *University Laboratory of Physiology, University of Oxford, Oxford OX1 3PT, UK*
[2] *School of Biomedical Sciences, University of Leeds, Leeds LS2 9JT, UK*
[3] *Medizinische Universitätsklinik Würzburg, 97080 Würzburg, Germany*

The majority of Na^+ channels in the heart are composed of the tetrodotoxin (TTX)-resistant (K_D, 2–6 μM) $Na_v1.5$ isoform; however, recently it has been shown that TTX-sensitive (K_D, 1–10 nM) neuronal Na^+ channel isoforms ($Na_v1.1$, $Na_v1.3$ and $Na_v1.6$) are also present and functionally important in the myocytes of the ventricles and the sinoatrial (SA) node. In the present study, in mouse SA node pacemaker cells, we investigated Na^+ currents under physiological conditions and the expression of cardiac and neuronal Na^+ channel isoforms. We identified two distinct Na^+ current components, TTX resistant and TTX sensitive. At 37°C, TTX-resistant i_{Na} and TTX-sensitive i_{Na} started to activate at ~ -70 and ~ -60 mV, and peaked at -30 and -10 mV, with a current density of 22 ± 3 and 18 ± 1 pA pF^{-1}, respectively. TTX-sensitive i_{Na} inactivated at more positive potentials as compared to TTX-resistant i_{Na}. Using action potential clamp, TTX-sensitive i_{Na} was observed to activate late during the pacemaker potential. Using immunocytochemistry and confocal microscopy, different distributions of the TTX-resistant cardiac isoform, $Na_v1.5$, and the TTX-sensitive neuronal isoform, $Na_v1.1$, were observed: $Na_v1.5$ was absent from the centre of the SA node, but present in the periphery of the SA node, whereas $Na_v1.1$ was present throughout the SA node. Nanomolar concentrations (10 or 100 nM) of TTX, which block TTX-sensitive i_{Na}, slowed pacemaking in both intact SA node preparations and isolated SA node cells without a significant effect on SA node conduction. In contrast, micromolar concentrations (1–30 μM) of TTX, which block TTX-resistant i_{Na} as well as TTX-sensitive i_{Na}, slowed both pacemaking and SA node conduction. It is concluded that two Na^+ channel isoforms are important for the functioning of the SA node: neuronal (putative $Na_v1.1$) and cardiac $Na_v1.5$ isoforms are involved in pacemaking, although the cardiac $Na_v1.5$ isoform alone is involved in the propagation of the action potential from the SA node to the surrounding atrial muscle.

(Resubmitted 25 May 2004; accepted after revision 12 July 2004; first published online 14 July 2004)
Corresponding author M. Lei: University Laboratory of Physiology, University of Oxford, Oxford OX1 3PT, UK. Email: ming.lei@physiol.ox.ac.uk

Under physiological conditions, the cardiac action potential originates in specialized pacemaker cells located in the centre of the SA node. The pacemaker activity of the SA node cells is due to the presence of a spontaneous diastolic depolarization (the pacemaker potential) that is driven by a net inward current. This net inward current results from the deactivation of outward current, i.e. delayed rectifier K^+ current (i_K), and the activation of inward currents, including Na^+-dependent background current ($i_{b,Na}$), hyperpolarization-activated current (i_f), T- and L-type Ca^{2+} currents ($i_{Ca,T}$, $i_{Ca,L}$) and, probably, the sustained inward current (i_{st}) (Irisawa *et al.* 1993; Boyett *et al.* 2000). Although inward voltage-dependent Na^+ current, i_{Na}, has been recorded from SA node cells (Brown, 1982; Nathan, 1986; Irisawa *et al.* 1993; Honjo *et al.* 1996), it is unclear whether it contributes to the pacemaker potential. For example, i_{Na} may be inactivated at the relatively positive potentials during the pacemaker potential in the SA node.

During the last decade, significant progress has been made in understanding the molecular basis of

*S. A. Jones and J. Liu contributed equally to this work.

DOI: 10.1113/jphysiol.2004.068643

voltage-gated Na^+ channels. They are composed of pore-forming α (Na_v) subunits and auxiliary β subunits (Catterall, 2000; Goldin *et al.* 2000; Goldin, 2001). Ten α subunits and four β subunits have been identified so far (Goldin, 2001; Yu & Catterall, 2003). Different α subunit isoforms are expressed in different tissues and have different pharmacological properties (Goldin, 2001). $Na_v1.5$ is mainly expressed in cardiac tissue and is inhibited by micromolar concentrations of tetrodotoxin (TTX), whereas $Na_v1.1$, $Na_v1.2$, $Na_v1.3$ and $Na_v1.6$ are mainly expressed in the central nervous system and are inhibited by nanomolar concentrations of TTX, as is the isoform expressed in skeletal muscle ($Na_v1.4$). However, a neuronal Na^+ channel ($Na_v1.1$) has been reported in the SA node in the newborn rabbit (Baruscotti *et al.* 1997*a*). Neuronal Na^+ channels are also present in the adult heart: multiple neuronal Na^+ channel isoforms ($Na_v1.1$, $Na_v1.3$, $Na_v1.6$), as well as $Na_v1.5$, are expressed in adult mouse ventricular myocytes and are involved in excitation–contraction coupling (Maier *et al.* 2002*b*). In another recent study, TTX-sensitive neuronal Na^+ channel isoforms have been shown to be expressed in the adult mouse and adult rat SA node and block of the channels has been shown to lead to a slowing of the heart rate in the isolated mouse heart (Maier *et al.* 2003). Although these recent studies highlight possible roles of neuronal Na^+ channels in the adult heart, including SA node pacemaking, Na^+ current through the channels has not been recorded under physiological conditions. Therefore, it is unclear whether the properties of neuronal Na^+ channels are appropriate for them to contribute to the relatively positive pacemaker potentials in SA node cells.

The aim of the present study was to study i_{Na} in adult mouse SA node cells. In isolated SA node cells, we have shown that both $Na_v1.1$ and $Na_v1.5$ can be expressed and there are corresponding TTX-sensitive and -resistant Na^+ currents. The TTX-sensitive (putative $Na_v1.1$) current has appropriate properties for it to be involved in the pacemaker potential. Experiments on the intact SA node show that $Na_v1.1$ and $Na_v1.5$ are both involved in pacemaking, but only $Na_v1.5$ is involved in action potential propagation.

Methods

Cell isolation

Cells were isolated from the mouse SA node based on the method for isolation of rabbit SA node cells previously described (Lei & Brown, 1996; Lei *et al.* 2002*a*,*b*). Briefly, 20–30 g C57BL/6J adult mice (age, 10–12 weeks; from Charles River UK Ltd, Kent, UK) were killed by cervical dislocation and the heart quickly removed and washed by Langendorff perfusion for 5–10 min using oxygenated Tyrode solution. All animal procedures were performed in accordance with the United Kingdom Animals (Scientific Procedures) Act, 1986. The right atrium was cut from the heart and placed in a dissection chamber perfused with Tyrode solution and illuminated from below. A thin strip of SA node tissue ($\sim$0.2 mm $\times$ 0.8 mm), limited by the crista terminalis, the atrial septum and the orifices of the venae cavae, was cut from the right atrium and allowed to regain spontaneous activity. The SA node tissue strip was incubated for 5 min in Ca^{2+}-free Tyrode solution, incubated for 20–30 min in enzyme-containing Ca^{2+}-free Tyrode solution (230 units ml^{-1} Type I collagenase; 15 units ml^{-1} Type IIA elastase; Sigma, Poole, UK) and, finally, washed and stored in Kraft-Brühe (KB) medium at 4°C for at least 1 h.

Whole-cell current and voltage clamp

Cells were superfused with Tyrode solution at 37°C at a rate of 2 ml min^{-1} via a heat exchanger. SA node cells were identified by their characteristic morphology and spontaneous activity. The whole-cell patch clamp technique was used for electrical recording from single cells with amphotericin-permeabilized or ruptured patches. Pipettes (tip diameter, $\sim$1–2 μm; resistance, 1–2 MΩ for ruptured patch and 2–5 MΩ for amphotericin-permeabilized patch) were made from 1 mm diameter glass (Clark Electromedical Instruments, Reading, UK) using a Narishige pipette puller (PP-830, Narishige Scientific Instruments Laboratory, Tokyo, Japan). Amphotericin 200 μg ml^{-1} was added to the pipette solution just before use. An Axopatch-200B patch clamp amplifier (Axon Instruments Inc., Union City, CA, USA) was used for current and voltage clamp. Cell capacitance (C_m) was obtained from the capacity compensation control of the amplifier after the whole-cell capacity current (in response to 5 ms pulses to $-$70 mV at 100 Hz from a holding potential of $-$60 mV) was eliminated. The series resistance was electronically compensated (> 80%) and the current signal was filtered by a low pass Bessel filter with a cut-off frequency of 5 kHz ($-$3 dB). Data were digitized at 1–2 kHz using a Digidata 1200A A/D converter (Axon Instruments Inc.) and stored on a computer for later analysis using pCLAMP version 8.2 software (Axon Instruments Inc.).

For action potential clamp, experiments were carried out, with some modifications, using the technique described by Doerr *et al.* (1989). In the current clamp mode, spontaneous action potentials were recorded for 30–60 s after a stable perforated whole-cell configuration was achieved. After switching to the voltage clamp mode, the pre-recorded action potentials were applied to the same cell as the command waveform.

Electrical mapping

Dissection of the intact SA node was carried out as previously described (Lei *et al.* 2001, 2002*a*). The preparation was superfused with Tyrode solution at 37°C at a rate of 5–6 ml min^{-1} via a heat exchanger. Extracellular potentials and intracellular action potentials were recorded by bipolar electrodes and conventional microelectrodes (resistance, ∼30 MΩ), respectively, as described by Yamamoto *et al.* (1998). Electrical signals were digitized at 5 kHz by a DigiData 1322A A/D converter (Axon Instruments Inc.) and stored on a computer for later analysis.

Solutions

Normal Tyrode solution (mM): 140 NaCl; 5.4 KCl; 1.8 $CaCl_2$; 1 $MgCl_2$; 10 glucose; 5 Hepes (pH 7.4 with NaOH). For recording i_{Na}, NaCl was reduced to 67 mM (NaCl replaced by CsCl) and 300 nM nisoldipine was added to solutions to block $i_{Ca,L}$; 40 μM NiCl was added to block $i_{Ca,T}$ in some experiments. KB solution (mM): 25 KCl; 0.5 EGTA; 3 $MgCl_2$; 80 L-glutamic acid; 20 taurine; 10 KH_2PO_4; 10 glucose; 10 Hepes (pH 7.4 with KOH). The pipette solution for ruptured whole-cell recording contained (mM): 10 NaCl; 140 KCl; 1 $MgCl_2$; 5 MgATP; 2 EGTA; 10 Hepes (pH 7.3 with KOH). The pipette solution for amphotericin-permeabilized whole-cell recording contained (mM): 140 KCl; 1.8 $MgSO_4$; 0.1 EGTA; 5 Hepes (pH 7.3 with KOH); prior to use, amphotericin was added as described above.

Immunocytochemistry

Immunocytochemistry was carried out on isolated cells and tissue sections as previously described (Musa *et al.* 2002). Ventricular and atrial cells were isolated as previously described (Ashley *et al.* 2002) and SA node cells were isolated as described above. Cells were plated onto collagen-treated slides and allowed to settle for 30 min. The intact SA node was dissected as previously described (Lei, 2001*b*, 2002) and then frozen. Tissue sections (8.0 μm; through the crista terminalis and the SA node) were cut perpendicular to the crista terminalis using a cryostat (Leica CM900, Wetzlar, Germany). Cells and sections were fixed in 10% formalin (Sigma) for 30 min, washed three times with phosphate buffer solution (PBS) over 30 min, permeabilized by 0.1% Triton X-100 (BDH, Poole, UK) for 30 min, washed three times with PBS over 30 min, and blocked with 1% bovine serum albumin (BSA; Sigma) and 10% normal donkey serum (Chemicon International, Temecula, CA, USA) in PBS for 1–2 h before application of primary antibody. Primary antibodies were diluted in 1% BSA and 2% normal donkey serum in PBS. Cells and sections were incubated with primary antibody (at an appropriate concentration) at 4°C overnight. Cells and sections were briefly washed in PBS and then FITC or Cy3-labelled donkey anti-rabbit or donkey anti-mouse secondary antibodies (Chemicon International) were applied. For double labelling, sections were incubated with a mixture of primary antibodies (raised in different species) and then an appropriate mixture of secondary antibodies. Cells and sections were washed three times with PBS and then mounted with Vectashield (H-1000 or H1300; Vector Laboratories, Peterborough, UK) and coverslips were sealed with nail polish. In control experiments on isolated cells and tissue sections, primary antibodies were preincubated with their antigenic peptides or no primary antibody was used and no labelling was detected.

Antibodies

Rabbit anti-connexin43 (Cx43; Sigma) was used at a dilution of 1 : 500; mouse anti-desmoplakin I and II (Progen, Heidelberg, Germany) was used as supplied; rabbit anti-HCN4 (Alomone Laboratories, Jerusalem, Israel) was used at a dilution of 1 : 100; rabbit anti-$Na_v1.1$, anti-$Na_v1.2$, anti-$Na_v1.3$, anti-$Na_v1.5$ and anti-$Na_v1.6$ (Alomone Laboratories) were used at a dilution of 1 : 50; rabbit anti-$Na_v1.5$ (kindly provided by Dr W. A. Catterall, University of Washington, Seattle, USA) was used at dilutions of 1 : 50 and 1 : 100. The specificity of anti-$Na_v1.1$, anti-$Na_v1.2$, anti-$Na_v1.3$, anti-$Na_v1.5$ and anti-$Na_v1.6$ was previously described (Planells-Cases *et al.* 2000; Malhotra *et al.* 2001; Maier *et al.* 2002*b*, 2003).

Confocal microscopy

Images were acquired using a confocal laser scanning microscope (LSM 510; Zeiss, Germany) equipped with argon and helium–neon lasers, which allowed excitation at 488 and 568 nm wavelengths for the detection of fluorescein isothiocyanate (FITC) and Cy3, respectively. The images recorded were single optical sections and, in the case of double labelling, the images were recorded sequentially. The images were saved and then processed using Corel Photo-Paint and Corel Draw software (Corel, Ottawa, Canada).

Statistical analysis

Data are presented as means ± S.E.M. (number of preparations or cells). Differences were evaluated by Student's *t* test and a difference was considered significant if $P < 0.05$.

Results

Isolation and characterization of TTX-sensitive and -resistant i_{Na} in mouse SA node cells

Cells from the SA node were identified by their characteristic size, shape and morphology as well as spontaneous electrical activity. Current was recorded during 20 ms pulses to potentials between −90 (or −70) and +30 mV from a holding potential of −120 (or −80) mV. i_{Na} was recorded in all SA node cells studied. In three cells (holding potential, −80 mV), the current was abolished by 30 μM TTX (sufficient to block both TTX-sensitive and -resistant Na^+ channels; data not shown). The current was also Na^+ dependent: in 67 mM Na^+ the peak current density was 40 ± 3 pA pF^{-1} (holding potential, −120 mV; $n = 9$), whereas in 140 mM Na^+ it was 74 ± 20 pA pF^{-1} (holding potential, −80 mV; $n = 6$) and 103 ± 13 pA pF^{-1} (holding potential, −120 mV; $n = 2$) (data not shown). These findings demonstrate that the current was indeed i_{Na}.

Dose–response curves for TTX block of i_{Na} were determined at test potentials of −60 and −10 mV from a holding potential of −120 mV; nanomolar to micromolar concentrations of TTX were used (three or four cells at each concentration were studied). At −60 mV, TTX-resistant cardiac $Na_v1.5$ channels are activated, whereas neuronal TTX-sensitive Na^+ channels are closed – they are activated at more positive potentials (Smith & Goldin, 1998; Zimmer *et al.* 2002*a*,*b*). At −10 mV, all Na^+ channel isoforms are activated. If cells contain both TTX-sensitive and -resistant Na^+ channels, dose–response curves should be different at the two test potentials with a deviation at nanomolar concentrations of TTX. The dose–response curves are shown in Fig. 1*B*. At TTX concentrations between 10 and 100 nM a significantly larger fraction of Na^+ channels were indeed blocked at a test potential of −10 mV compared to a test potential of −60 mV. The difference between the dose–response curves was not the result of a voltage-dependent block of $Na_v1.5$, because the heterologously expressed $Na_v1.5$ channel exhibits an indistinguishable block at both potentials (T. Zimmer, personal communication). These results suggest that two components of i_{Na}, TTX sensitive and resistant, exist in mouse SA node cells. The dose–response curve at −60 mV is well fitted with a Hill curve (with a Hill coefficient of 1) with a K_D of 0.4 μM (Fig. 1*B*). This is consistent with published values of the K_D for TTX-resistant i_{Na} (2–6 μM; Goldin, 2001). The dose–response curve at −10 mV is well fitted with a double Hill curve (Fig. 1*B*): if it is assumed that the K_D of TTX-resistant current is 0.4 μM (and the Hill coefficients of both TTX-resistant and -sensitive currents is 1), the K_D of the TTX-sensitive current is 2.2 nM (and the fractions of TTX-resistant and -sensitive currents are 0.7 and 0.3, respectively). The K_D of the TTX-sensitive current is consistent with published values (1–10 nm; Goldin, 2001).

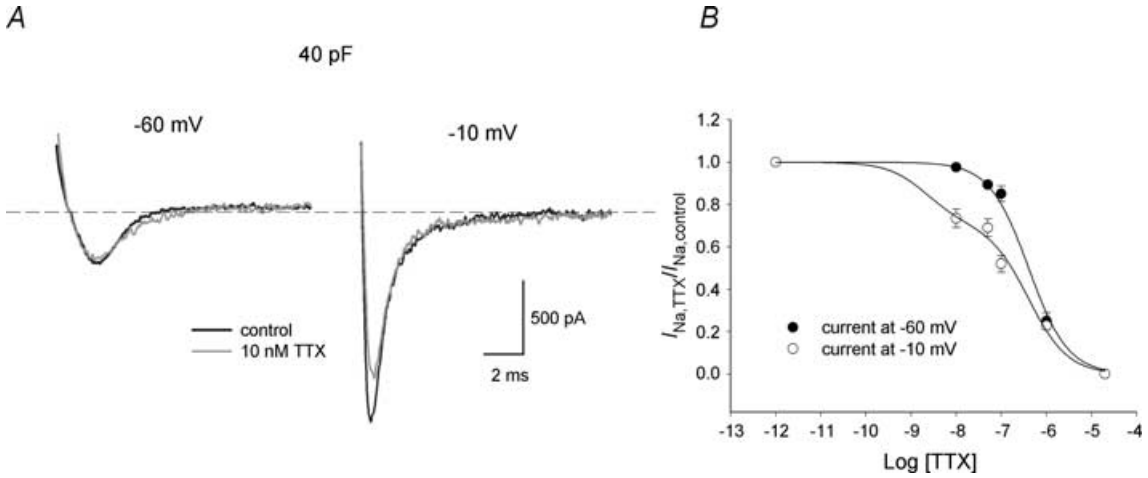

Figure 1. Dose–response curves for TTX block of i_{Na}
A, current recorded at test potentials of −60 and −10 mV from holding potential of −120 mV under control conditions and in the presence of 10 nM TTX in a SA node cell. *B*, dose–response curves for TTX block of i_{Na} at test potentials of −60 and −10 mV. Means ± S.E.M. ($n = 3$–4). The data are fitted with a Hill-type curve:

$$b = 1 - \left(\frac{m[\mathrm{TTX}]}{K_{D,s} + [\mathrm{TTX}]}\right) - \left(\frac{(1-m)[\mathrm{TTX}]}{K_{D,r} + [\mathrm{TTX}]}\right),$$

where b is the fractional block of total i_{Na}, m is TTX-sensitive i_{Na} as a fraction of total i_{Na} (zero at −60 mV and 0.3 at −10 mV), [TTX] is the TTX concentration, $K_{D,s}$ is the dissociation constant of TTX-sensitive i_{Na} (2.2 nM) and $K_{D,r}$ is the dissociation constant of TTX-resistant i_{Na} (0.4 μM).

i_{Na} subtypes were characterized according to their sensitivity to TTX. Figure 2*A–H* shows families of i_{Na} recordings under control conditions and in the presence of 10 nM to 20 μM TTX (holding potential, −120 mV). According to the TTX sensitivity of TTX-sensitive i_{Na} and TTX-resistant i_{Na} (see above), 10 nM TTX should block TTX-sensitive i_{Na} without effect on TTX-resistant i_{Na}; 100 nM TTX should block TTX-sensitive i_{Na}, with little effect on TTX-resistant i_{Na}; the current remaining in the presence of > 100 nM TTX should be only TTX-resistant i_{Na}. The current blocked by 10 and 100 nM TTX (obtained by subtraction; TTX-sensitive i_{Na}) is shown in Fig. 2*C* and *E*. The current remaining in the presence of 100 nM and 1 μM TTX (TTX resistant i_{Na}) is shown in Fig. 2*D* and *F*. Activation curves were constructed for TTX-sensitive and -resistant i_{Na} (Fig. 2*I*) and were fitted by the Boltzmann equation, $a = 1/\{1 + \exp[(V_m - V_{1/2})/k]\}$, where a is the activation variable, V_m is the membrane potential, $V_{1/2}$ is the potential at which the current is half-activated and k is the slope factor. TTX-sensitive i_{Na} was activated at more positive potentials than TTX-resistant i_{Na}: the $V_{1/2}$ and k values for activation are -29 ± 1 and 8.4 ± 0.7 mV for TTX-sensitive i_{Na} blocked by 10 nM TTX, -30 ± 2 and 8.5 ± 1 mV for TTX-sensitive i_{Na} blocked by 100 nM TTX, -44 ± 4 and 7 ± 2 mV for TTX-resistant i_{Na} recorded in the presence of 100 nM TTX, and -45 ± 1 and 6 ± 1 mV for TTX-resistant i_{Na} recorded in the presence of 1 μM TTX. Thus two distinct currents with different activation characteristics can be isolated by their sensitivity to TTX. This is the first evidence of two distinct Na^+ currents in adult SA node.

Figure 2*J* shows the current–voltage relationships for total i_{Na}, TTX-sensitive i_{Na} and TTX-resistant i_{Na} constructed from current recorded under control conditions, current blocked by 100 nM TTX and current in the presence of 100 nM TTX. At body temperature, total i_{Na}, TTX-sensitive i_{Na} and TTX-resistant i_{Na} started to activate at ∼ −70, ∼ −60 and ∼ −70 mV, and peaked at −20, −10 and −30 mV, with a current density of 40 ± 3, 18 ± 1 and 22 ± 3 pA pF^{-1}, respectively ($n = 9$; cell capacitance, $C_m = 30$–55 pF). There was a substantial variation in the density of i_{Na} from cell to cell. Cells in the centre of the SA node are small as compared to those in the periphery (Boyett *et al.* 2000). The capacitance (C_m; a measure of cell size) of 11 cells studied varied from 30 to 61 pF and there was a significant correlation between the density of total i_{Na} and C_m (R^2, 0.59; $P < 0.05$) and the density of TTX-resistant i_{Na} and C_m (R^2, 0.57; $P < 0.05$), but not between the density of TTX-sensitive i_{Na} and C_m (Fig. 2*K*). This suggests that the density of TTX-resistant, but not TTX-sensitive, i_{Na} may vary from the centre to the periphery of the SA node. Note that for small cells (presumably from the centre of the SA node), the densities of TTX-resistant and -sensitive i_{Na} were approximately equal, but in large cells (presumably from the periphery of the SA node) the density of TTX-resistant i_{Na} was much greater than the density of TTX-sensitive i_{Na}.

Inactivation curves for TTX-sensitive (current blocked by 100 nM TTX) and -resistant (current recorded in the presence of 100 nM TTX) i_{Na} were constructed using a standard double pulse protocol (holding potential, −120 mV; conditioning pulse potential, −120 to −20 mV; conditioning pulse duration, 100 ms; conditioning pulse–test pulse interval, 0 ms; test pulse potential, −30 mV; test pulse duration, 10 ms; conditioning–test pulse repetition rate, 2 Hz). Figure 2*L–N* shows families of test pulse currents for total i_{Na}, TTX-resistant i_{Na} and TTX-sensitive i_{Na} and Fig. 2*O* shows inactivation curves for TTX-sensitive and -resistant i_{Na}. Inactivation curves were fitted by the Boltzmann equation as described above. The $V_{1/2}$ and k values for inactivation were -56 ± 2 and 3 ± 1 mV for TTX-sensitive i_{Na} and -65 ± 5 and 6 ± 1 mV for TTX-resistant i_{Na}. The activation and inactivation curves overlap (corresponding to window current) (Fig. 2*O*) – the overlap for TTX-sensitive i_{Na} occurs at more positive potentials than for TTX-resistant i_{Na} (Fig. 2*O*).

To explore the role of TTX-sensitive i_{Na}, action potential clamp experiments were successfully conducted on three cells. Figure 3 shows a representative experiment. The action potentials in Fig. 3*A* were recorded in current-clamp mode before switching to voltage clamp, and were used as the command waveform in the same cell for current recording. After a steady pattern of current was obtained under control conditions (Fig. 3*B*), 50 nM TTX was applied (sufficient to block TTX-sensitive i_{Na}, with little effect on TTX-resistant i_{Na}). This resulted in an increase in the net outward current due to block of the TTX-sensitive inward current during the action potential. The change in current was not due to rundown, because the current returned to the control pattern after wash-off of TTX (not shown). The TTX-sensitive current during the action potential was obtained by subtracting current in the presence of TTX from the control current (Fig. 3*D*). The action potential command waveform and the TTX-sensitive current are shown at a fast time base in Fig. 3*E*. Figure 3*E* shows that the TTX-sensitive current (i_{Na}) started late during diastole. The current–voltage relationship in Fig. 3*F* (in which the TTX-sensitive current is plotted against the membrane potential during the action potential command waveform) shows that the TTX-sensitive current started to activate at ∼ −50 mV. This is consistent with the threshold of the TTX-sensitive i_{Na} measured with square voltage clamp pulses (Fig. 2*I*). Figure 3*F* also shows that the TTX-sensitive current reached a peak during the action potential upstroke and was inactivated by the peak of the action potential. This is the first time TTX-sensitive i_{Na} has been recorded under action potential clamp.

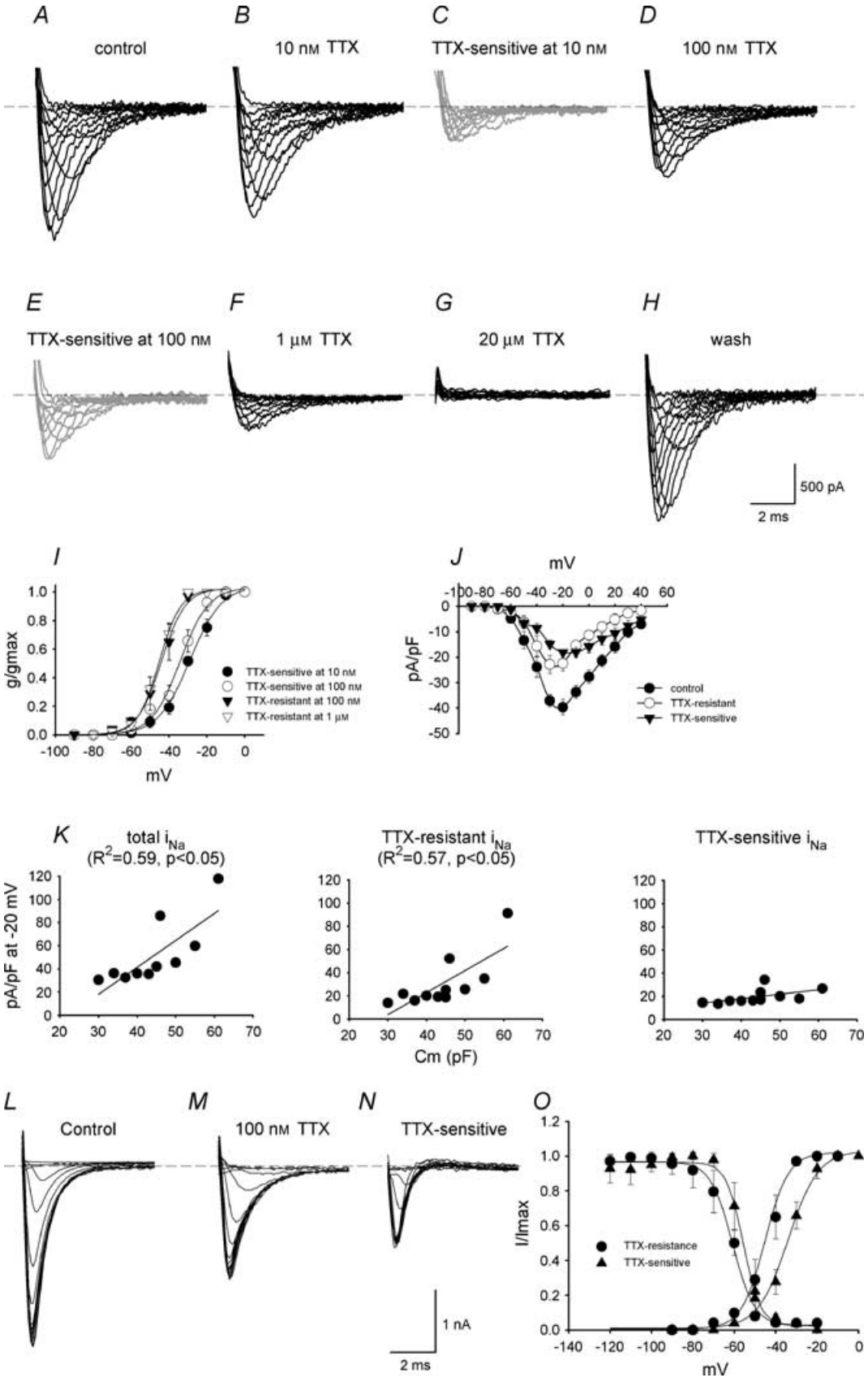

Expression of Na^+ channel isoforms in mouse SA node cells

To examine the molecular basis of TTX-sensitive and -resistant i_{Na}, ~100 isolated SA node cells were immunolabelled for $Na_v1.1$, $Na_v1.2$, $Na_v1.3$, $Na_v1.5$ and $Na_v1.6$. Figure 4 shows punctate labelling of the TTX-sensitive $Na_v1.1$ along the cell membrane of small (Fig. 4*A*) and large (Fig. 4*B*) SA node cells. Nuclear labelling by anti-$Na_v1.1$ was also observed – this presumably was non-specific labelling. There was labelling of the TTX-resistant $Na_v1.5$ along the cell membrane in large (Fig. 4*F*), but not small (Fig. 4*E*), SA node cells (labelling of $Na_v1.5$ in ventricular and atrial cells is also shown in Fig. 4*C* and *D*). No labelling of $Na_v1.2$ was observed in SA node cells (Fig. 4*G* and *H*). Figure 4*I* shows labelling of $Na_v1.2$ in brain tissue – this proves that the antibody used is effective. No labelling of $Na_v1.3$ was observed in SA node cells (Fig. 4*J* and *K* shows labelling of $Na_v1.3$ in brain tissue). Finally, no labelling of $Na_v1.6$ was observed in SA node cells (Fig. 4*L* and *M*).

We also characterized the expression pattern of $Na_v1.1$ and $Na_v1.5$ in tissue sections. Figure 5*B*–*E* shows sections cut half-way between the superior and inferior venae cavae (approximate position of the leading pacemaker site). The sections were cut through the crista terminalis (largely atrial muscle), the intercaval region, and the interatrial septum (atrial muscle). In the SA node of the rabbit, the centre of the SA node is located in the intercaval region and the periphery of the SA node extends up the endocardial face of the crista terminalis (Boyett *et al.* 2003). $Na_v1.1$ and $Na_v1.5$ were immunolabelled, but, in addition, connexin43 (Cx43), desmoplakin and HCN4 were immunolabelled as markers. Cx43 is a gap junction protein and is known to be present in atrial muscle and the periphery of the SA node, but absent from the centre of the SA node (Boyett *et al.* 2003). Desmoplakin is a component of desmosomes (which provide mechanical coupling between cells) and is present in all myocytes (atrial muscle and SA node). HCN4 is the principal isoform responsible for the hyperpolarization-activated channel and is known to be present throughout the SA node, but not in atrial muscle (Boyett *et al.* 2003). Figure 5*B* shows that, whereas desmoplakin signal (red) was present throughout the section, Cx43 signal (green) was absent from the intercaval region adjacent to the crista terminalis. The Cx43-negative region corresponds to the centre of the SA node. Figure 5*C* shows that HCN4 signal was present in the centre of the SA node in the intercaval region, but not in the atrial muscle of the crista terminalis and towards the interatrial septum. Figure 5*C* shows that HCN4 signal was also present on the endocardial surface of the crista terminalis; this presumably corresponds to the periphery of the SA node. Cx43 signal was present on the endocardial surface of the crista terminalis (data not shown); it is known that Cx43 is expressed in the periphery of the rabbit SA node (Boyett *et al.* 2003). The use of Cx43, desmoplakin and HCN4 therefore allows the centre and periphery of the SA node to be identified. Figure 5*D* shows that $Na_v1.5$ signal was present throughout the section except for the centre of the SA node at the foot of the crista terminalis. In contrast, $Na_v1.1$ signal was present throughout the tissue including the centre and periphery of the SA node (Fig. 5*E*). Figure 5*E* shows that, in the mouse SA node, the periphery of the SA node on the endocardial surface of the crista terminalis can be separated from the atrial muscle of the crista terminalis by connective tissue (as it is in the rabbit SA node; Boyett *et al.* 2003). In summary, based on the expression of Cx43, desmoplakin, HCN4, $Na_v1.5$ and $Na_v1.1$, three tissue types were identified (SA node centre, SA node periphery, atrial muscle); the distribution of the tissues is summarized schematically in Fig. 5*A* and the expression of proteins, including $Na_v1.5$ and $Na_v1.1$, in these tissues is summarized by the table in Fig. 5.

Effect of TTX on mouse SA node pacemaking and conduction

To address the roles of the TTX-sensitive and -resistant i_{Na} in SA node pacemaking, nanomolar or micromolar concentrations of TTX were applied to intact SA node preparations and isolated SA node cells. Under control

Figure 2. Characteristics of TTX-sensitive and -resistant i_{Na}
A–H, recordings of current under control conditions (total i_{Na}; *A*), current in the presence of 10 nM TTX (*B*), current blocked by 10 nM TTX (obtained by subtraction; TTX-sensitive i_{Na}; *C*), current in the presence of 100 nM TTX (TTX-resistant i_{Na}; *D*), current blocked by 100 nM TTX (obtained by subtraction; TTX-sensitive i_{Na}; *E*), current in the presence of 1 μM TTX (*F*), current in the presence of 20 μM TTX (*G*) and current after wash-off of TTX (*H*) (C_m, 45 pF). *I*, activation curves for TTX-sensitive (blocked by 10 or 100 nM TTX) and -resistant (in the presence of 100 nM or 1 μM TTX) i_{Na}. Means ± S.E.M. ($n = 3$ at 10 nM and 1 μM TTX, $n = 9$ at 100 nM TTX). *J*, current–voltage relationships for total i_{Na}, TTX-sensitive i_{Na} (blocked by 100 nM TTX) and TTX-resistant i_{Na} (in the presence of 100 nM TTX). Means ± S.E.M. ($n = 9$). *K*, densities of total i_{Na}, TTX-resistant i_{Na} (in the presence of 100 nM TTX) and TTX-sensitive i_{Na} (blocked by 100 nM TTX) plotted against C_m. The data are fitted with straight lines as a result of linear regressions (R^2 and *P* values shown). *L–N*, recordings of total i_{Na}, TTX-resistant i_{Na} (in the presence of 100 nM TTX) and TTX-sensitive i_{Na} (blocked by 100 nM TTX) during the test pulse of the inactivation protocol (C_m, 45 pF). *O*, activation and inactivation curves for TTX-sensitive (blocked by 100 nM TTX) and -resistant (in the presence of 100 nM TTX) i_{Na}. Means ± S.E.M. ($n = 6$–9).

conditions, the intact SA node preparations showed regular spontaneous activity with a cycle length of 178 ± 4 ms ($n = 22$). Figure 6 shows typical examples of extracellular potentials and action potentials recorded in and around the SA node (Fig. 6*A*) and a typical activation map (Fig. 6*B*). Spontaneous action potentials were initiated in the centre of the SA node and from here they propagated to the crista terminalis and the interatrial septum (Fig. 6*A* and *B*). Figure 6*C* shows extracellular potentials from the centre and periphery of the SA node (recording sites 'a' and 'b' in Fig. 6*B*) in the presence of different concentrations of TTX. TTX at 10 and 100 nM resulted in significant increases in the cycle length of $6 \pm 2\%$ (from 175 ± 5 ms to 187 ± 3 ms; $P < 0.05$, $n = 4$) and $22 \pm 8\%$ (from 184 ± 6 to 221 ± 18 ms; $P < 0.05$, $n = 6$). TTX at 30 μM caused a greater increase in the cycle length at the leading pacemaker site in the centre of the SA node of $44 \pm 13\%$ from 158 ± 8 to 240 ± 22 ms ($P < 0.01$, $n = 5$). These results suggest that rate is approximately equally dependent on TTX-sensitive and -resistant i_{Na}: of the increase in cycle length produced by block of both currents by 30 μM TTX, ~51% was produced by block of TTX-sensitive i_{Na} alone by 100 nM TTX. Although pacemaking at the leading pacemaker site in the centre of the SA node persisted in micromolar concentrations of TTX, in all preparations ($n = 6$) 10–30 μM TTX abolished activity in the peripheral region of the SA node (Fig. 6*C*).

Figure 6*D* shows extracellular potentials from the centre of the SA node and the neighbouring atrial muscle (recording sites 'a' and 'c' in Fig. 6*B*). This permits measurement of SA node conduction time (time taken for conduction from 'a' to 'c' in Fig. 6*B*). TTX at 10 nM ($n = 4$) and 100 nM ($n = 6$) caused no significant change of SA node conduction. However, as shown in Fig. 6*D*, 1 and 5 μM TTX prolonged SA node conduction by 106 ± 44

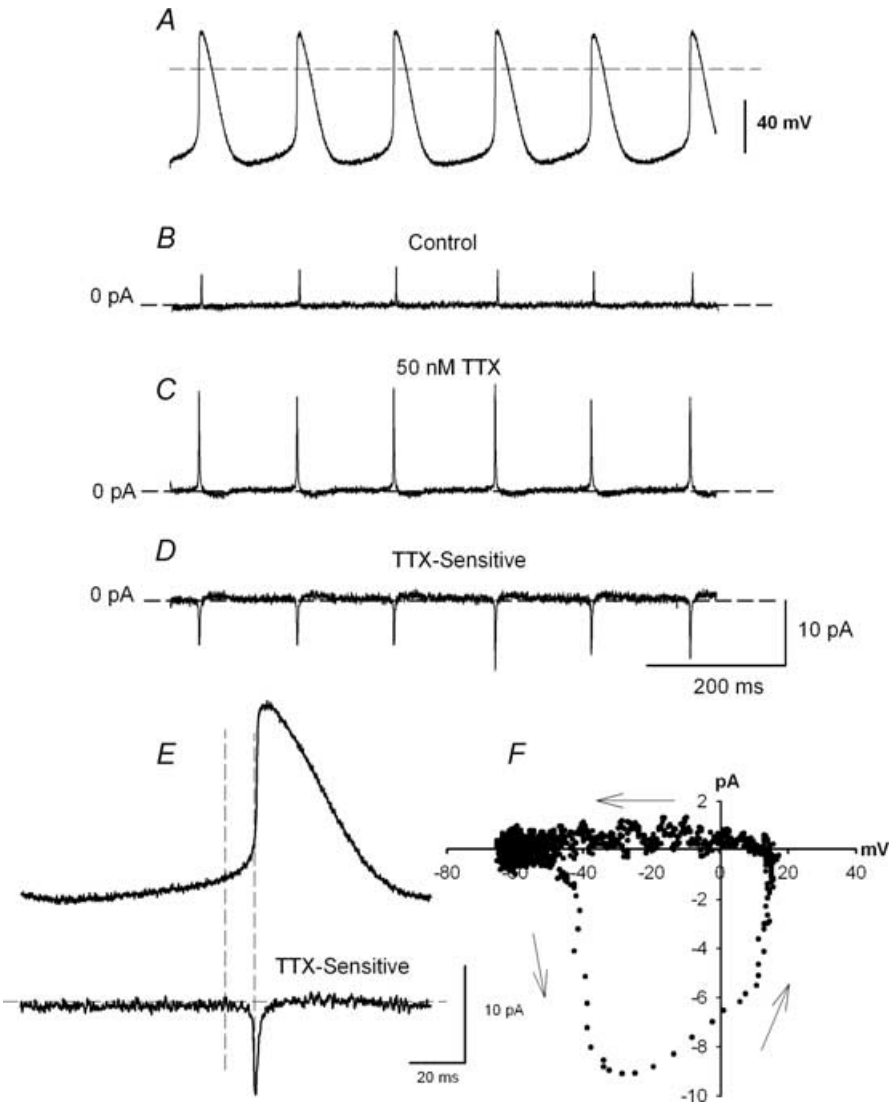

Figure 3. Action potential clamp recording of TTX-sensitive i_{Na}
A, spontaneous action potentials used as voltage clamp command waveform in the same cell. *B*, current recorded under control conditions. *C*, current recorded during superfusion of 50 nM TTX. *D*, TTX-sensitive current (obtained by subtracting *C* from *B*). *E*, action potential command waveform and the TTX-sensitive current at a fast time base. *F*, current–voltage relationship of TTX-sensitive i_{Na} obtained from *E* (the TTX-sensitive current is plotted against the membrane potential).

and $226 \pm 58\%$ ($P < 0.01$, $n = 5$). (Under control conditions, the SA node conduction time was 10.3 ± 0.5 ms, $n = 17$.) TTX at 10 μM caused 3 : 1 or 2 : 1 SA node conduction block (Fig. 6*C*) and 30 μM TTX blocked SA node conduction (Fig. 6*C*). These results suggest that SA node conduction is controlled by TTX-resistant i_{Na} and not TTX-sensitive i_{Na}.

The effect of TTX on the spontaneous electrical activity of isolated SA node cells was also investigated. A typical example is shown in Fig. 7 and mean data are shown in Table 1. Block of both TTX-sensitive and -resistant i_{Na} by 30 μM TTX reduced the slope of the pacemaker potential and the threshold potential, and increased cycle length (Table 1). Approximately 63% of the effect of block of both TTX-sensitive and -resistant i_{Na} by 30 μM TTX on cycle length can be attributed to block of TTX-sensitive i_{Na} alone (the effect caused by 100 nM TTX). This confirms that rate is dependent on both TTX-sensitive and -resistant i_{Na}. Block of both currents by 30 μM TTX also decreased the maximum upstroke velocity and the peak of the action potential (Table 1). Approximately 49% of the decrease in the maximum upstroke velocity, but just ~12% of the decrease in the peak of the action potential, can be attributed to block of TTX-sensitive i_{Na} alone. This result suggests that TTX-resistant i_{Na} plays an equal or greater role than TTX-sensitive i_{Na} in the action potential upstroke. Action potential conduction is dependent on the peak of the action potential (as well as the maximum

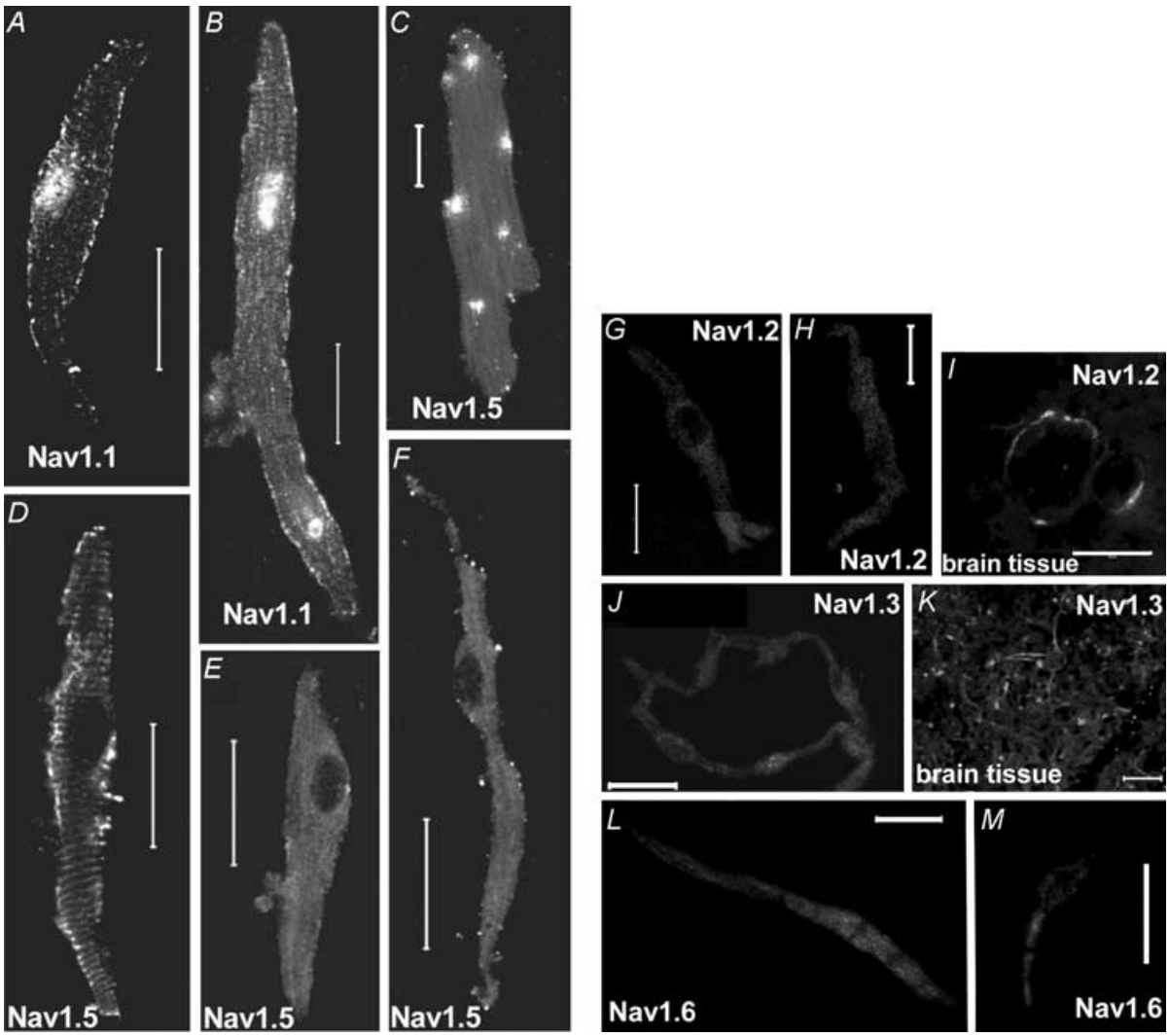

Figure 4. Labelling of $Na_v1.1$, $Na_v1.2$, $Na_v1.3$, $Na_v1.5$ and $Na_v1.6$ in isolated cardiac cells and brain tissue
A and *B*, labelling of $Na_v1.1$ in small (*A*) and large (*B*) SA node cells. *C–F*, labelling of $Na_v1.5$ in ventricular (*C*), atrial (*D*) and small (*E*) and large (*F*) SA node cells. *G–I*, absence of labelling of $Na_v1.2$ in SA node cells (*G* and *H*) and labelling of $Na_v1.2$ in brain tissue (*I*). *J* and *K*, absence of labelling of $Na_v1.3$ in SA node cells (*J*) and labelling of $Na_v1.3$ in brain tissue (*K*). *L* and *M*, absence of labelling of $Na_v1.6$ in SA node cells. Scale bars, 20 μm.

Table 1. Effect of 100 nM and 30 μM TTX on the action potential of isolated SA node cells

	Control	100 nM TTX[a]	% change	Control	30 μM TTX[b]	% change
Slope of pacemaker potential (mV s^{-1})	219 ± 12	149 ± 11**	−31 ± 6	227 ± 5	148 ± 14**	−35 ± 5
Threshold potential (mV)	−46 ± 1	−41 ± 0.4**	11 ± 3	−44 ± 2	−38 ± 1*	13 ± 4
Cycle length (ms)	157 ± 2	184 ± 4**	17 ± 2	168 ± 5	207 ± 5**	27 ± 4
Maximum upstroke velocity (mV s^{-1})	48 ± 3	35 ± 5**	−24 ± 13	50 ± 3	25 ± 2**	−49 ± 7
Peak of action potential (mV)	35 ± 6	33 ± 4	−4 ± 2	37 ± 5	25 ± 4*	−33 ± 1

[a]$n = 6$; C_m, 28–58 pF; [b]$n = 5$; C_m, 27–46 pF. Absolute values (means ± S.E.M.) and percentage changes from control are shown. Asterisks show significant differences from control: *$P < 0.05$, **$P < 0.01$.

upstroke velocity) and the dependence of the peak of the action potential on TTX-resistant i_{Na} could help explain the dependence of SA node conduction on TTX-resistant i_{Na}.

Discussion

This study shows for the first time two distinct Na^+ currents coexisting in adult SA node pacemaker cells, a TTX-sensitive i_{Na} and a TTX-resistant i_{Na}. As well

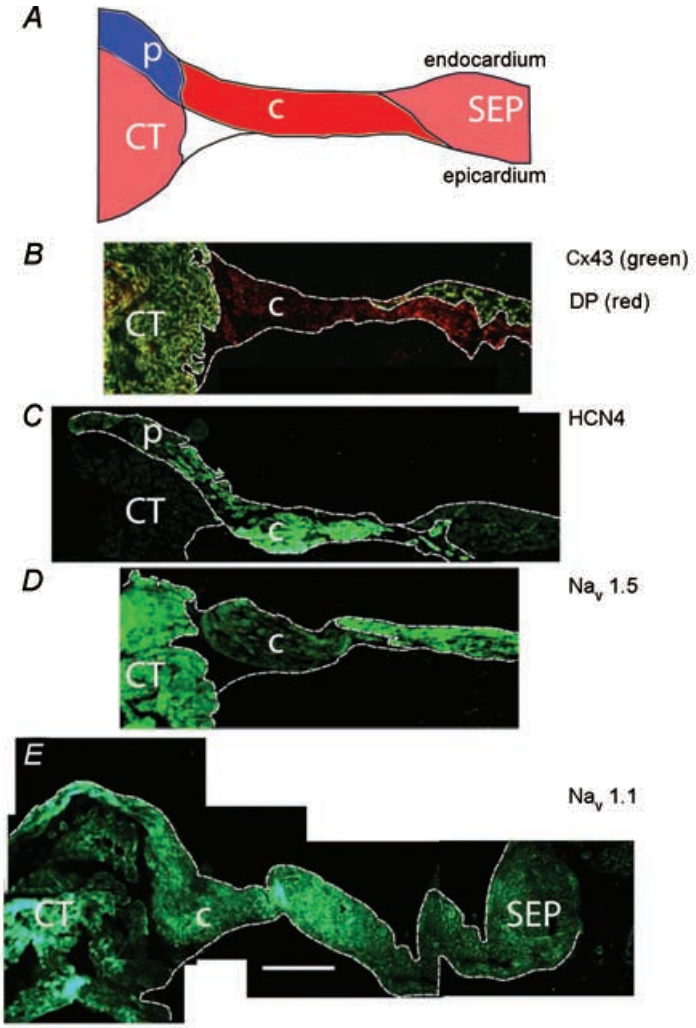

	Cx43	Desmoplakin	HCN4	Na$_v$1.5	Na$_v$1.1
SA node centre (c)	-	+	+	-	+
SA node periphery (p)	+	+	+	+	+
Crista terminalis (CT) and interatrial septum (SEP)	+	+	-	+	+

Figure 5. Labelling of Cx43, desmoplakin, HCN4, Na$_v$1.5 and Na$_v$1.1 in SA node sections
A, schematic diagram of a section. *B*, double labelling of Cx43 (green) and desmoplakin (DP; red). *C*, labelling of HCN4. *D*, labelling of Na$_v$1.5. *E*, labelling of Na$_v$1.1. Table: summary of the expression of the different proteins in the regions shown in *A*. Scale bars, 200 μm.

as different TTX sensitivities, the two Na^+ currents have a different voltage dependence of activation and inactivation, a different cell size dependence and different roles in the SA node.

Na^+ channel isoforms in the SA node

Recent studies have shown that $Na_v1.5$ is not the only Na^+ channel isoform in the adult heart and neuronal isoforms are also present (Maier *et al.* 2002*b*, 2003). Using mouse and rat tissue sections, Maier *et al.* (2003) showed that $Na_v1.5$ is absent from the centre of SA node, whereas $Na_v1.1$ is expressed throughout the SA node and surrounding atrial muscle (expression of $Na_v1.1$ mRNA has also been shown in newborn rabbit SA node; Baruscotti *et al.* 1997*b*). Using single cells (for the first time) and tissue sections, these findings are confirmed here. In addition, in the present study, it is shown that the distribution of

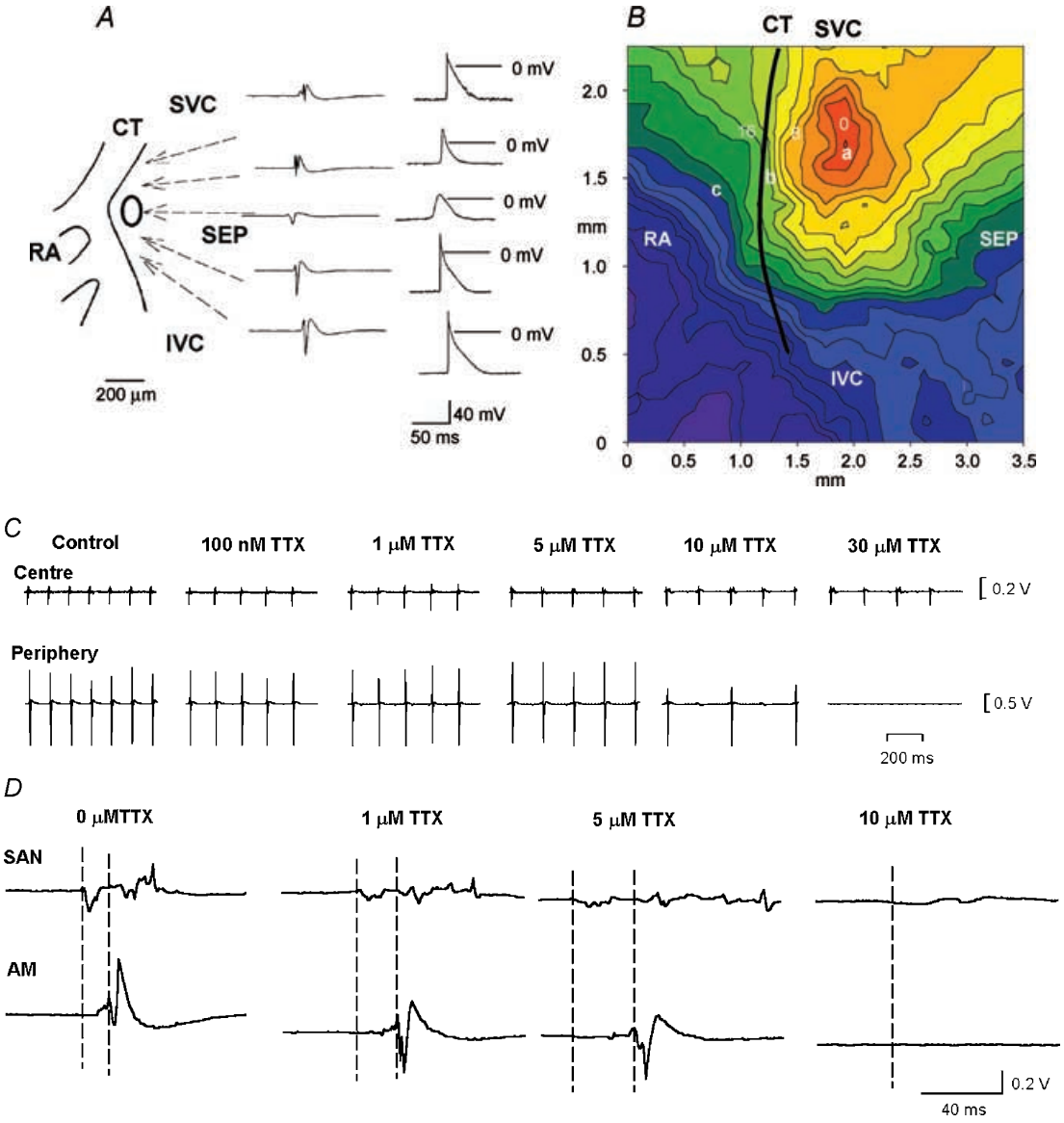

Figure 6. Effect of TTX on SA node pacemaking and conduction
A, extracellular potentials (left) and action potentials (right) recorded in and around the SA node. *B*, activation sequence of the SA node under control conditions. Isochrones at 2 ms intervals and activation times in milliseconds are shown. *C*, effect of TTX on SA node pacemaking. Extracellular potentials recorded from sites 'a' (centre of the SA node) and 'b' (periphery of the SA node) in *B* are shown. *D*, effect of TTX on SA node conduction. Extracellular potentials from sites 'a' (leading pacemaker site in the centre of the SA node, SAN) and 'c' (atrial muscle, AM) are shown. Vertical dashed lines indicate the time of initiation of the action potential at the leading pacemaker site (left) and the arrival of the action potential in the atrial muscle. SVC, superior vena cava; SEP, interatrial septum; IVC, inferior vena cava; RA, right atrial appendage; CT, crista terminalis. All extracellular potentials amplified (by 10^4).

$Na_v1.5$ is complex: although $Na_v1.5$ was not expressed in small SA node cells (likely to be from the centre of the SA node) and in the region of the SA node located in the intercaval region (the centre), it was expressed in large SA node cells (likely to be from the periphery of the SA node) and in the region of the SA node located on the endocardial face of the crista terminalis (the periphery) (Figs 4 and 5).

$Na_v1.3$ has also been reported in sections of mouse SA node (Maier *et al.* 2003), but not in rabbit and rat SA node (Baruscotti *et al.* 1997*b*; Maier *et al.* 2003). However, in the present study, we did not observe the expression of $Na_v1.3$ in isolated mouse SA node cells, and in tissue sections labelling of $Na_v1.3$ was only observed in nerve fibres and nerve cell bodies within and near the SA node (data not shown), which is known to be highly innervated. Labelling of $Na_v1.3$ in nerve fibres and nerve cell bodies was also observed in rat SA node by Maier *et al.* (2003). The discrepancy in $Na_v1.3$ labelling in mouse SA node between the two studies could be the result of a difference in the mouse strain used (B6/129F1 mice were used by Maier *et al.* 2003, while C57BL/6J mice were used in the present study) or a difference in the protocol used.

Although neuronal Na^+ channels have been detected in adult heart, including the SA node, Na^+ current through these channels had not been recorded under physiological conditions. In the present study, we determined dose–response curves for TTX block of i_{Na} in isolated mouse SA node cells as shown in Fig. 1. At TTX concentrations between 10 and 100 nM we observed a significantly greater block of i_{Na} at −10 mV compared to that at −60 mV. The difference between the dose–response curves at −10 and −60 mV suggests that two components of i_{Na} exist in these cells. i_{Na} was separated into two distinct components, TTX sensitive and TTX resistant, by their sensitivity to TTX (Fig. 2*A*–*H*). TTX-sensitive i_{Na} activated and peaked at more positive potentials compared to TTX-resistant i_{Na} (Fig. 2*J*) and the $V_{1/2}$ of activation and inactivation of TTX-sensitive i_{Na} was more positive as compared to that of TTX-resistant i_{Na} (Fig. 2*I* and *O*). These differences are in principle consistent with the properties of different Na^+ channels when they are expressed exogenously: Mantegazza *et al.* (2001) have shown that the $Na_v1.5$ channel activates at a potential 20 mV more negative than the neuronal $Na_v1.2$ channel (the voltage dependence of activation of $Na_v1.1$ and $Na_v1.2$ is the same; Smith & Goldin, 1998). Furthermore, all neuronal Na^+ channels, including $Na_v1.1$, are known to have a more positive voltage dependence of inactivation than $Na_v1.5$ (Goldin, 1999): $Na_v1.5$ inactivates at a potential 25 mV more negative than $Na_v1.1$.

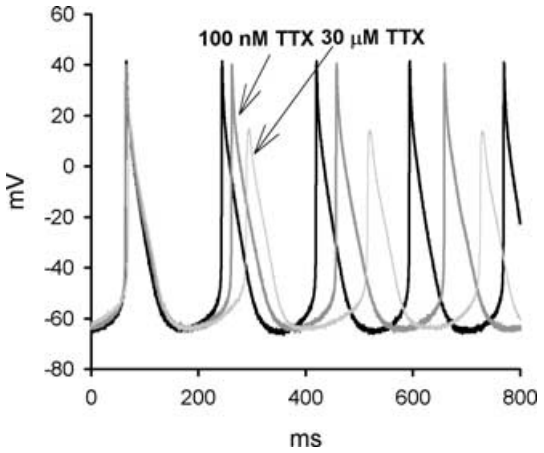

Figure 7. The effect of TTX on spontaneous electrical activity of an isolated SA node cell
Spontaneous actions potentials of a SA node cell (C_m, 35 pF) under control conditions, after 2 min exposure to 100 nM TTX and after a further 2 min application of 30 μM TTX.

Our results show that the density of total i_{Na} varies in mouse SA node cells and density is significantly correlated with cell size and is greater in larger cells (Fig. 2*K*). This appears to be the result of variation in the density of TTX-resistant i_{Na} with cell size, because the density of TTX-sensitive i_{Na} did not vary with cell size (Fig. 2*K*). Because cells in the centre of the SAN are known to be smaller than those in the periphery (Boyett *et al.* 2000), this suggests that the density of TTX-resistant i_{Na} (but not TTX-sensitive i_{Na}) declines from the periphery to the centre of the SA node. This is consistent with the distributions of $Na_v1.5$ and $Na_v1.1$ as determined by immunolabelling: whereas $Na_v1.5$ was not expressed in the centre of the SA node, it was expressed in the periphery; in contrast, $Na_v1.1$ was expressed throughout the SA node and surrounding atrial muscle (see above and Figs 4 and 5).

Roles of Na^+ channel isoforms in SA node pacemaking

Previously, i_{Na} was not thought to play an important role in SA node pacemaking (Brown, 1982; Irisawa *et al.* 1993). However, this study and the study of Maier *et al.* (2003) have shown that block of TTX-sensitive neuronal Na^+ channels by 100 nM TTX slows down pacemaking: the cycle length was increased in mouse intact heart by ∼65% (Maier *et al.* 2003), mouse intact SA node by 22 ± 8% (present study) and mouse isolated SA node cells by 15 ± 2% (present study). This suggests that TTX-sensitive neuronal Na^+ channels play a role in SA node pacemaking. In the SA node, the centre, made up of small cells, is normally the leading pacemaker site. The TTX-sensitive Na^+ channel, $Na_v1.1$, is present throughout the SA node, including the centre (this study; Maier *et al.* 2003) and, in the present study, in isolated SA node cells TTX-sensitive i_{Na} was present in

large and small cells and the density of the current did not vary with cell size (Fig. 2*K*). TTX-sensitive i_{Na}, more than TTX-resistant i_{Na}, has properties appropriate for SA node pacemaking: at the relatively positive potentials (~ -60 mV) during the pacemaker potential, a greater fraction of TTX-sensitive i_{Na} than TTX-resistant i_{Na} will be available, because the inactivation curve of TTX-sensitive i_{Na} is shifted to more positive potentials as compared to that of TTX-resistant i_{Na} (Fig. 2*I*). In addition, because of overlap of the activation and inactivation curves there is expected to be window current for both TTX-sensitive and -resistant i_{Na}. However, window current in the case of TTX-sensitive i_{Na} is available at more positive potentials (perhaps more appropriate for pacemaking) than window current in the case of TTX-resistant i_{Na} (Fig. 2*O*). In the present study, action potential clamp experiments confirmed that TTX-sensitive i_{Na} activated during diastolic depolarization (Fig. 3). In the present study, block of TTX-resistant i_{Na} as well as TTX-sensitive i_{Na} by 30 μM TTX resulted in an extra slowing of pacemaking as compared to block of TTX-sensitive i_{Na} alone by nanomolar concentrations of TTX in both the intact SA node and isolated SA node cells. This suggests that TTX-resistant i_{Na}, as well as TTX-sensitive i_{Na}, plays a role in SA node pacemaking. Although the properties of $Na_v1.5$ are less appropriate for pacemaking, there can be a greater density of TTX-resistant i_{Na} than TTX-sensitive i_{Na} (Fig. 2*K*) and this perhaps explains its importance. Even in the presence of 30 μM TTX, pacemaking continued in intact SA node preparations (Fig. 6*C*) and isolated SA node cells (Fig. 7) and this shows that currents other than i_{Na} are involved in pacemaking.

Roles of Na^+ channel isoforms in SA node conduction

Block of both TTX-sensitive and -resistant i_{Na} by micromolar concentrations of TTX, but not block of the TTX-sensitive i_{Na} alone by 10 or 100 nM TTX, caused a slowing of SA node conduction (from the leading pacemaker site in the centre of the SA node to the surrounding atrial muscle via the periphery of the SA node) or even SA node conduction block (Fig. 6*D*). This shows an important role for TTX-resistant i_{Na} in SA node conduction. i_{Na} is expected to control conduction, because the conduction velocity depends on both the upstroke velocity and amplitude of the action potential and both of these are dependent on i_{Na} (Fig. 7). The SA node conduction time, as measured in this study, will primarily depend on the periphery of the SA node and, in the periphery of the SA node, the dominant i_{Na} is likely to be the TTX-resistant i_{Na} (in large SA node cells, likely to be from the periphery, the density of TTX-resistant i_{Na} was greater than that of TTX-sensitive i_{Na}; Fig. 2*K*). This can explain the dependence of SA node conduction on TTX-resistant i_{Na}. Micromolar concentrations of TTX abolished activity in the periphery, but not the centre, of the SA node. This is probably because the action potential upstroke in the periphery, but not the centre, is dependent on i_{Na}, whereas in the centre, it is dependent on $i_{Ca,L}$ (Kodama *et al.* 1997).

Physiological and clinical importance

The present study shows that Na^+ channels play an important role in the functioning of the SA node and this is borne out by independent work. In the present study, block of TTX-resistant i_{Na} (presumably through the $Na_v1.5$ channel) resulted in a slowing of SA node pacemaking, a slowing of SA node conduction and SA node exit block (Fig. 6). These are symptoms of sick sinus syndrome (Benditt *et al.* 1990). In a study of the SA node from heterozygous *Scn5a* (gene for $Na_v1.5$) knockout mice, a sick sinus syndrome phenotype was observed (unpublished data). Knockout of the Na^+ channel $\beta 2$ subunit also results in a sick sinus syndrome phenotype (Maier *et al.* 2002*a*). Recently, a case of familial sick sinus syndrome in a patient was ascribed to a mutation in *SCN5A* (Benson *et al.* 2003).

In conclusion, two distinct Na^+ channels are expressed in the SA node. Both neuronal and cardiac Na^+ channels contribute to the initiation of the action potential in the SA node and, in addition, the cardiac Na^+ channel is also responsible for the propagation of the action potential out of the SA node.

References

Ashley EA, Sears CE, Bryant SM, Watkins HC & Casadei B (2002). Cardiac nitric oxide synthase 1 regulates basal and β-adrenergic contractility in murine ventricular myocytes. *Circulation* **105**, 3011–3016.

Baruscotti M, Westenbroek R, Catterall WA, DiFrancesco D & Robinson RB (1997*a*). The newborn rabbit sino-atrial node expresses a neuronal type I-like Na^+ channel. *J Physiol* **498**, 641–648.

Benditt D, Milstein S & Goldstein M (1990). Sinus node dysfunction: Pathophysiology, clinical features, evalution, and treatment. In *Cardiac Electrophysiology. From Cell to Bedside*, ed. Zips DP & Jalife J, pp. 708–734. W.B. Saunders, Philadelphia.

Benson DW, Wang DW, Dyment M, Knilans TK, Fish FA, Strieper MJ, Rhodes TH & George AL Jr (2003). Congenital sick sinus syndrome caused by recessive mutations in the cardiac sodium channel gene (SCN5A). *J Clin Invest* **112**, 1019–1028.

Boyett MR, Dobrzynski H, Lancaster MK, Jones SA, Honjo H & Kodama I (2003). Sophisticated architecture is required for the sinoatrial node to perform its normal pacemaker function. *J Cardiovasc Electrophysiol* **14**, 104–106.

Boyett MR, Honjo H & Kodama I (2000). The sinoatrial node, a heterogeneous pacemaker structure. *Cardiovasc Res* **47**, 658–687.

Brown HF (1982). Electrophysiology of the sinoatrial node. *Physiol Rev* **62**, 505–530.

Catterall WA (2000). From ionic currents to molecular mechanisms: the structure and function of voltage-gated sodium channels. *Neuron* **26**, 13–25.

Doerr T, Denger R & Trautwein W (1989). Calcium currents in single SA nodal cells of the rabbit heart studied with action potential clamp. *Pflugers Arch* **413**, 599–603.

Goldin AL (1999). Diversity of mammalian voltage-gated sodium channels. *Ann N Y Acad Sci* **868**, 38–50.

Goldin AL (2001). Resurgence of sodium channel research. *Annu Rev Physiol* **63**, 871–894.

Goldin AL, Barchi RL, Caldwell JH, Hofmann F, Howe JR, Hunter JC, Kallen RG, Mandel G, Meisler MH, Netter YB, Noda M, Tamkun MM, Waxman SG, Wood JN & Catterall WA (2000). Nomenclature of voltage-gated sodium channels. *Neuron* **28**, 365–368.

Honjo H, Boyett MR, Kodama I & Toyama J (1996). Correlation between electrical activity and the size of rabbit sino-atrial node cells. *J Physiol* **496**, 795–808.

Irisawa H, Brown HF & Giles W (1993). Cardiac pacemaking in the sinoatrial node. *Physiol Rev* **73**, 197–227.

Kodama I, Nikmaram MR, Boyett MR, Suzuki R, Honjo H & Owen JM (1997). Regional differences in the role of the Ca^{2+} and Na^+ currents in pacemaker activity in the sinoatrial node. *Am J Physiol* **272**, H2793–H2806.

Lei M & Brown HF (1996). Two components of the delayed rectifier potassium current, I_K, in rabbit sino-atrial node cells. *Exp Physiol* **81**, 725–741.

Lei M, Cooper P, Camelliti P & Kohl P (2002*a*). Contribution of the fast sodium inward current, iNa, to murine sino-atrial node pacemaking. *Biophys J* **82**, 605a.

Lei M, Cooper P, Camelliti P & Kohl P (2002*b*). Role of the 293b-sensitive, slowly activating delayed rectifier potassium current, i(K_s), in pacemaker activity of rabbit isolated sino-atrial node cells. *Cardiovas Res* **53**, 68–79.

Lei M, Honjo H, Kodama I & Boyett MR (2001). Heterogeneous expression of expression of the delayed-rectifier K^+ currents $i_{K,r}$ and $i_{K,s}$ in rabbit sinoatrial node cells. *J Physiol* **535**, 703–714.

Maier SK, Westenbroek RE, Chen C, Marble DR, Feigl EO, Isom LL, Catterall WA & Scheuer T (2002*a*). The β2-subunit of voltage-gated sodium channels is required for maintenance of regular sinus rhythm in the heart. *Biophys J* **82**, 609a.

Maier SK, Westenbroek RE, Schenkman KA, Feigl EO, Scheuer T & Catterall WA (2002*b*). An unexpected role for brain-type sodium channels in coupling of cell surface depolarization to contraction in the heart. *Proc Natl Acad Sci U S A* **99**, 4073–4078.

Maier SK, Westenbroek RE, Yamanushi TT, Dobrzynski H, Boyett MR, Catterall WA & Scheuer T (2003). An unexpected requirement for brain-type sodium channels for control of heart rate in the mouse sinoatrial node. *Proc Natl Acad Sci U S A* **100**, 3507–3512.

Malhotra JD, Chen C, Rivolta I, Abriel H, Malhotra R, Mattei LN, Brosius FC, Kass RS & Isom LL (2001). Characterization of sodium channel α- and β-subunits in rat and mouse cardiac myocytes. *Circulation* **103**, 1303–1310.

Mantegazza M, Yu FH, Catterall WA & Scheuer T (2001). Role of the C-terminal domain in inactivation of brain and cardiac sodium channels. *Proc Natl Acad Sci U S A* **98**, 15348–15353.

Musa H, Dobrzynski H, Berry Z, Abidi F, Cass CE, Young JD, Baldwin SA & Boyett MR (2002). Immunocytochemical demonstration of the equilibrative nucleoside transporter rENT1 in rat sinoatrial node. *J Histochem Cytochem* **50**, 305–309.

Nathan RD (1986). Two electrophysiologically distinct types of cultured pacemaker cells from rabbit sinoatrial node. *Am J Physiol* **250**, H325–H329.

Planells-Cases R, Caprini M, Zhang J, Rockenstein EM, Rivera RR, Murre C, Masliah E & Montal M (2000). Neuronal death and perinatal lethality in voltage-gated sodium channel alpha II-deficient mice. *Biophys J* **78**, 2878–2891.

Smith RD & Goldin AL (1998). Functional analysis of the rat I sodium channel in Xenopus oocytes. *J Neurosci* **18**, 811–820.

Yamamoto M, Honjo H, Niwa R & Kodama I (1998). Low-frequency extracellular potentials recorded from the sinoatrial node. *Cardiovasc Res* **39**, 360–372.

Yu FH & Catterall WA (2003). Overview of the voltage-gated sodium channel family. *Genome Biol* **4**, 207.

Zimmer T, Biskup C, Dugarmaa S, Vogel F, Steinbis M, Bohle T, Wu YS, Dumaine R & Benndorf K (2002*a*). Functional expression of GFP-linked human heart sodium channel (hH1) and subcellular localization of the a subunit in HEK293 cells and dog cardiac myocytes. *J Membr Biol* **186**, 1–12.

Zimmer T, Bollensdorff C, Haufe V, Birch Hirschfeld E & Benndorf K (2002*b*). Mouse heart Na^+ channels: primary structure and function of two isoforms and alternatively spliced variants. *Am J Physiol Heart Circ Physiol* **282**, H1007–H1017.

Acknowledgements

We thank Dr P. Kohl for support in performing the experiments and Dr R. Westenbroek for optimizing immunocytochemical procedures. We are grateful to Drs W. A. Catterall and T. Scheuer for helpful discussions. This work was supported by the Wellcome Trust and the British Heart Foundation. M.L. is a Wellcome Trust Career Development Fellow.